Supplement of Hydrol. Earth Syst. Sci., 26, 4251–4263, 2022
https://doi.org/10.5194/hess-26-4251-2022-supplement

Hydrology and Earth System Sciences
Open Access

Supplement of

A multivariate-driven approach for disentangling the reduction in near-natural Iberian water resources post-1980

Amar Halifa-Marín et al.

Correspondence to: Pedro Jiménez-Guerrero (pedro.jimenezguerrero@um.es)

Further information about NENWIRES dataset

For the Spanish Ministry of Environment (currently called *Ministerio para la Transición Ecológica y Reto Demográfico*) these series thus represent the official dataset of drained streamflow to the country reservoirs. Water inflows are estimated from the reservoir outflow while accounting for reservoir storage changes at daily scale. The computation of water inflows is conducted by two procedures. The first method to estimate the water inflows is calculated as follows (Eq. S1):

$$Awi = Pwr - Awr + Awo \qquad \text{(Eq. S1)}$$

where the Actual Water Inflows (Awi) are estimated by the subtraction of the Previous Water Reserve (PWR) adding the Actual Water Outputs. The 'Actual' records refer to the target month and 'Previous' records to the last month.

Likewise, the second method to estimate the water inflows is calculated as follows (Eq. S2):

$$Awi = Awr - Pwr + Awo \qquad \text{(Eq. S2)}$$

where the Actual Water Inflows (Awi) are estimated by the subtraction of the Previous Water Reserve (PWR) adding the Actual Water Outputs. The 'Actual' records refer to the target month and 'Previous' records to the last month.

The type of water inflow estimation depends on the time when the measurements are done. The type 1 (Eq. 1) mentions the reservoirs where the balance between water reserve and water outputs is done at the morning (more or less at 11 am). Meanwhile, the type 2 (Eq. 2) is used in reservoirs where the balance is done at the night (more or less at 11 pm).

We wish, however, to add a few clarifications about methods used to estimate the water inflows series collected in the NENWIRES dataset. First, water outflows refer to human-induced water reductions in the reserve (e.g. ecological flow, channels) but do not quantify evaporation and infiltration processes. The method of quantifying water inflows also should be impacted by the sediment accumulation rates in reservoirs, especially for limestones/clays environments. Given the well-known reduction of erosion processes as consequence of agricultural abandonment and dominant natural greening-up in the Iberian headwaters, we think that this method to assess the water inputs is robust. Besides we always found similar evolutions and trend magnitudes for water inflows between adjoining NENWIRES basins (under different conditions, as permeability/soils and basin dimension). In addition, small dams related to flood risk control or hydropower production were allowed within the criteria 1. As well as the basins are clearly still influenced by non-natural land use changes such as agricultural abandonment. Likewise, Basque, Balearic/Canary Islands, Galician, Catalonian, and Andalusian Basins were not studied (13% of Spanish territory) due to records are collected by local agencies. Despite all these drawbacks, near-natural water inputs series offer long-term estimations of streamflow to expanding the knowledge about water generation in Iberian headwaters where the existing data still is scarce.

Preprocessing data procedures

On the other hand, processing of NetCDF files for climate data was conducted with CDO software (Schulzweida, 2019). For converting from daily to seasonal scale (large winter, DJFM), seassum and seasmean CDO functions were used. After calculating the large winter accumulation of WP and average of maximum and minimum temperatures (WTX and WTN, respectively), its spatial average within the target watersheds is computed. This procedure was implemented in RCRAN language, loading the NetCDF files with the brick function (Hijmans, 2021). In addition, the catchments polygons (ESRI shapefile) were read with the readOGR function (Bivand, 2021). Then the gridded climate data is cropped within the boundaries of catchments using the mask function, and consecutively the spatial average of timesteps is estimated with the cellStats function (Hijmans, 2021). The extended winter accumulation/average of record series (WWI and NAOi) was also developed in RCRAN.

Figures

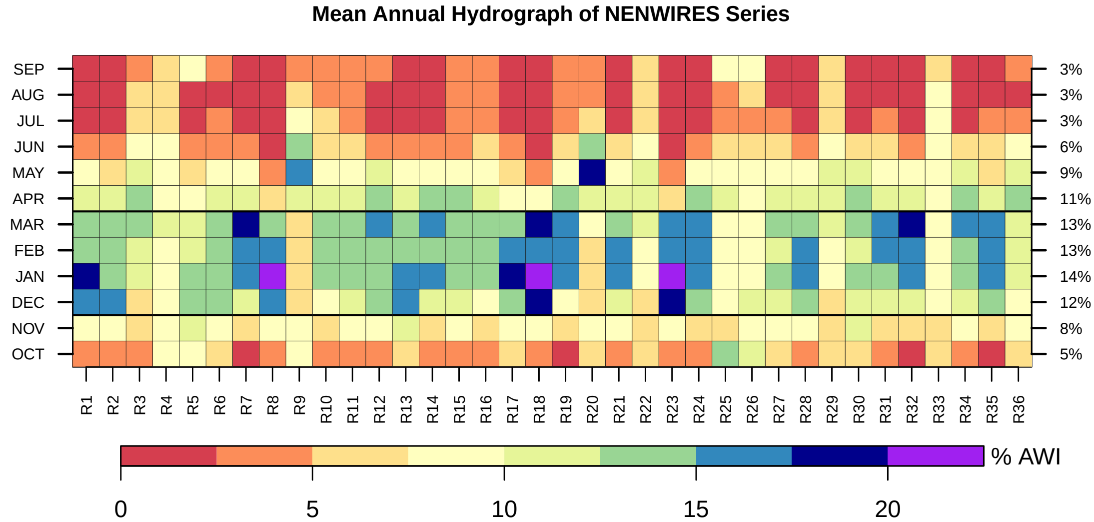

Figure S1. Novel hydrograph version for NENWIRES series. Each cell in the matrix shows the relative monthly contribution (rows) to the annual accumulation (AWI) in each NENWIRES catchment (columns). The monthly contribution is based on records along the study period. The monthly average of the dataset is highlighted in the right axis. The horizontal black lines highlight the extended wintertime season (DJFM).

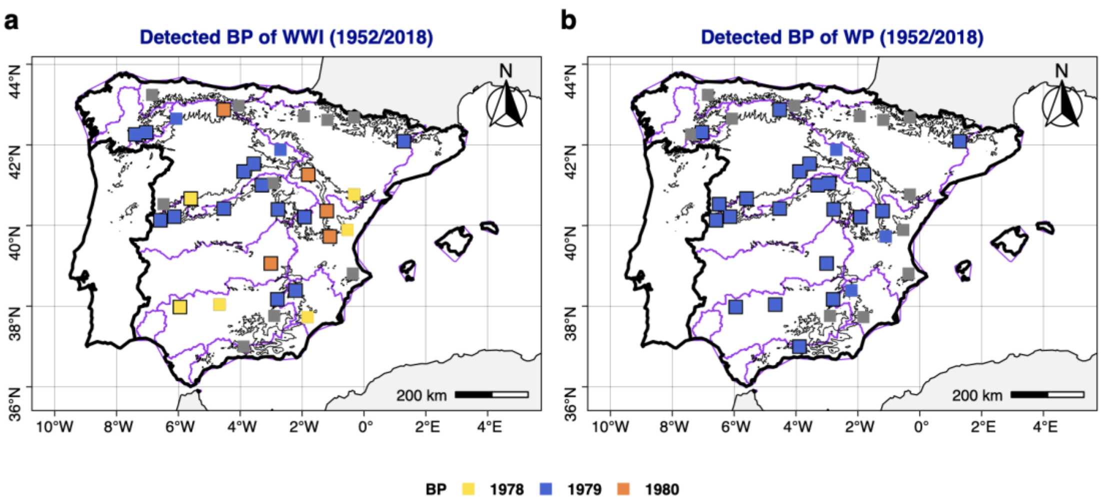

Figure S2. (a) Break point (BP) detected for WP series, and (b) Id. for WWI series through methods used in Fig. 3 of the manuscript. Grey squares represent a BP not detected between 1978 and 1980. Larger squares (framed into black borders) represent the significantly BP detected in both panels. Contours of orography (black) and IHB of continental Spain (purple) were also added (see Fig. 1).

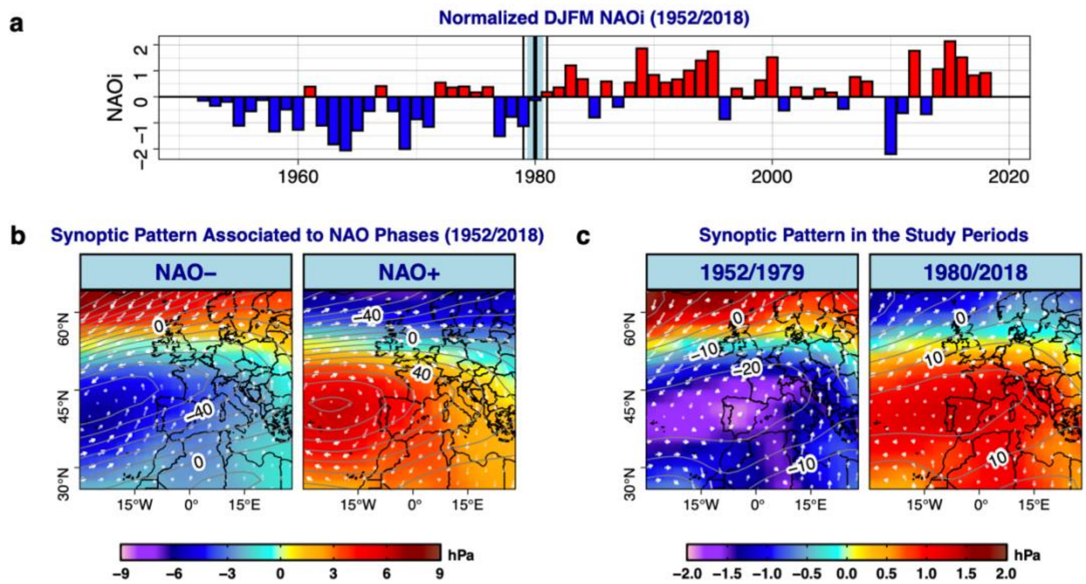

Figure S3. Panels show (a) Standardized wintertime NAOi (average of large winter, DJFM) and its detected BP (through methods shown in Fig. 3 of the manuscript); (b) the synoptic pattern based on NAO+/NAO- phases registered in the study period; and (c) similarly for the study periods 1952/1979 and 1980/2018. Synoptic patterns refer to the composite of SLP (painted), Z500 (numbered grey contours) and U/V-W speed/direction (white arrows). In case of white arrows, a greater size represents higher wind speed and arrows point to the wind direction. Country boundaries are also drawn (black contours). The source of this climate variables is the NCEP/NCAR Reanalysis 1, which has been widely used in many meteorological studies. It provides 2.5x2.5º global climate data framed between 90ºN/S latitude. The high quality of this reanalysis dataset in the northern hemisphere is due to the high density of the meteorological observations worldwide. The temporal coverage ranges from January 1948 to nearly real-time. NCEP/NCAR datasets were downloaded from the NOAA/PSL Website.

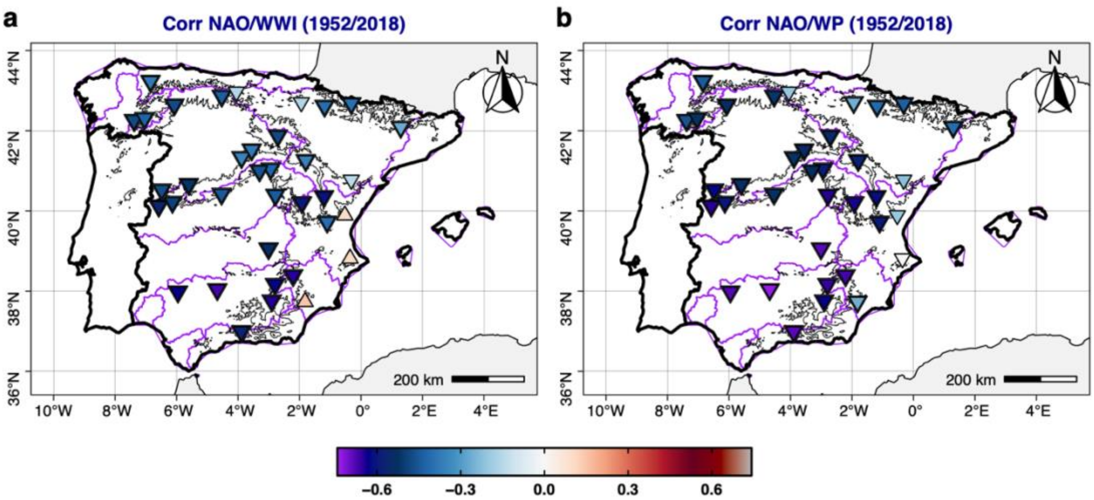

Figure S4. The wintertime correlation between NAOi and (a) precipitation; and (b) water inflows in the NENWIRES basins. Symbols represent positive correlation (filled triangle point-up) and negative correlation (filled triangle point down), being marked with a black outline the significant estimates. Contours of orography (black) and Iberian Hydrological Basins (IHB) of continental Spain (purple) were also added (see Fig. 1 of manuscript).

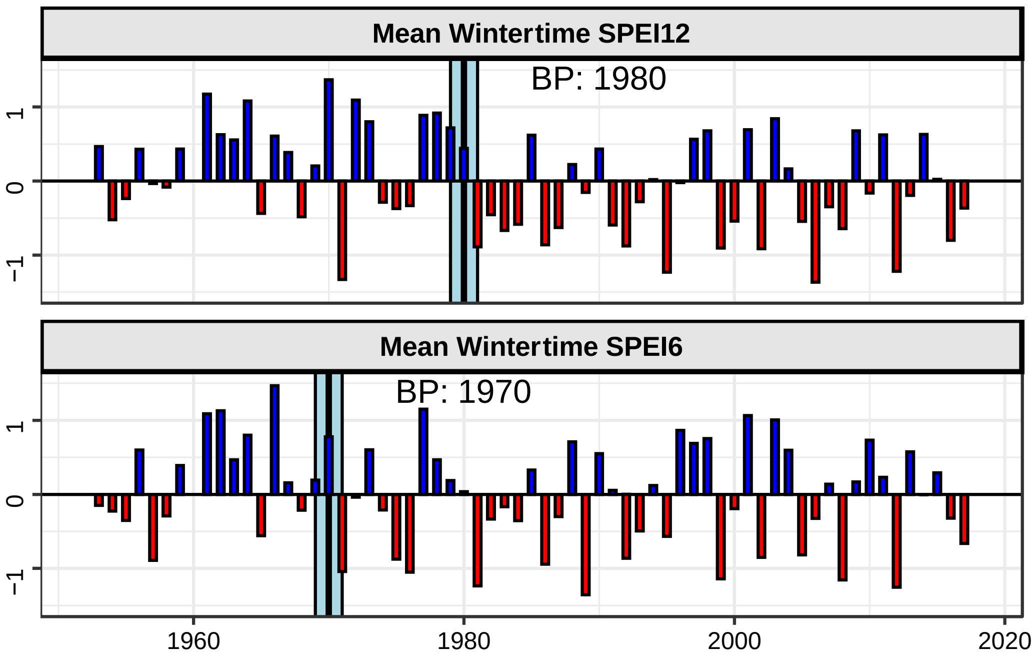

Figure S5. (a) Mean wintertime SPEI12 registered in the NENWIRES catchments (top) and (b) SPEI6 (bottom). The SPEI indices are computed from March (last month of the extended winter). Blue(red) bars represent positive(negative) estimations. The most likely change point (BP), computed through the methods used in Fig. 3 of the manuscript, is shown for both series (light blue and dark lines).

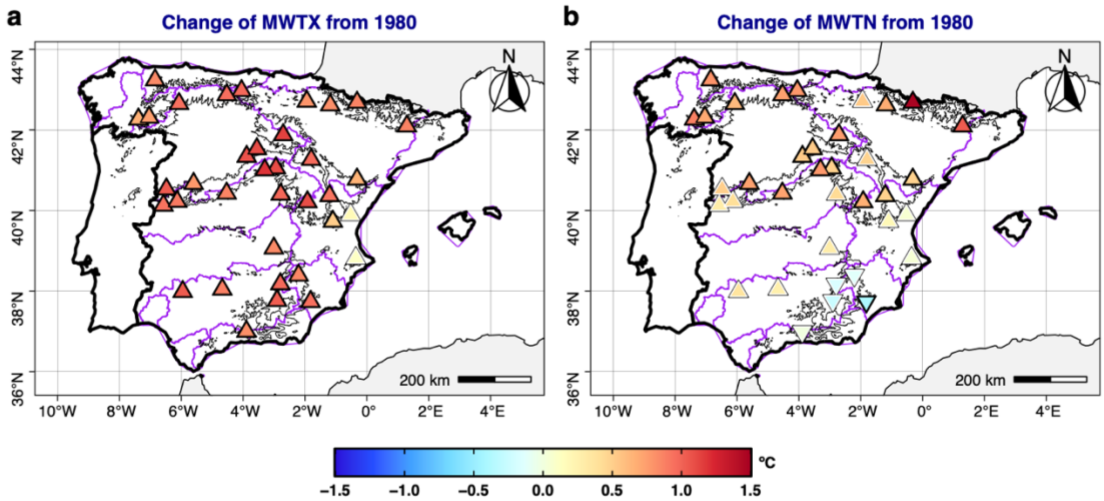

Figure S6. The wintertime absolute change of (a) maximum temperature (TMX); and (b) minimum temperature (TMN) from 1980 in the NENWIRES basins. Seasonal mean computed by TMX and TMN estimations at daily scale. Symbols represent increases (filled triangle point-up) and decreases (filled triangle point down), being marked with a black outline the significant estimates. Contours of orography (black) and IHB of continental Spain (purple) were also added (see Fig. 1 of manuscript).

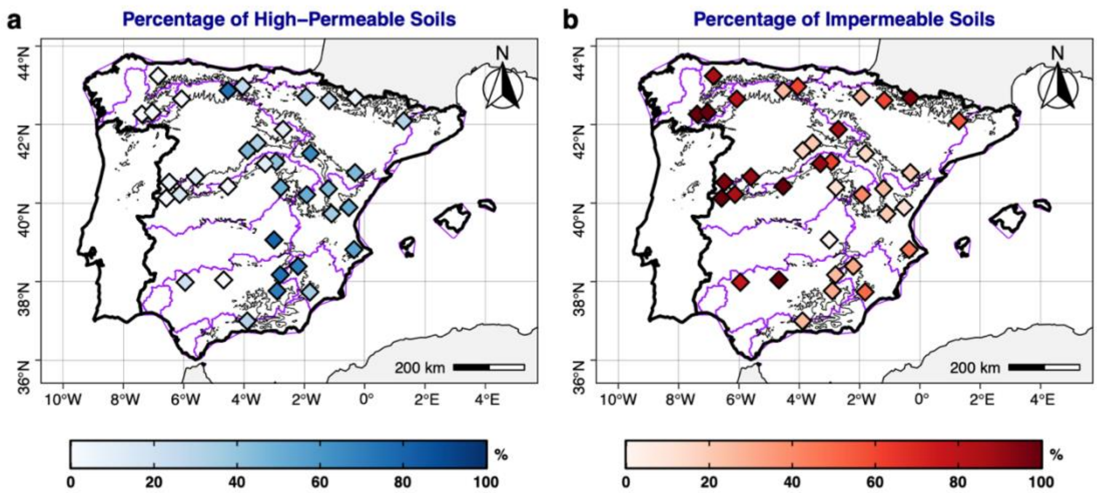

Figure S7. Percentage (%) of (a) high-permeable soils and (b) impermeable soils. See section 2.1 in the manuscript for further details about type of soils grouped in both cases. Contours of orography (black) and IHB of continental Spain (purple) were also added (see Fig. 1 of manuscript).

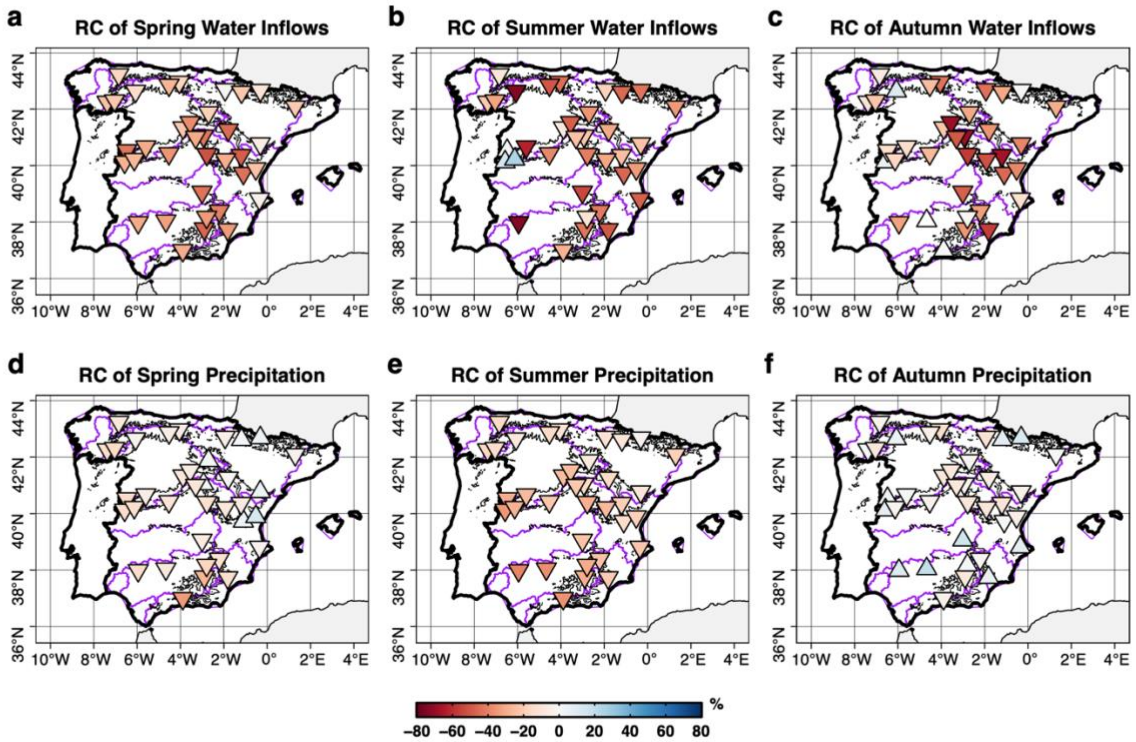

Figure S8. (a, b, c) Relative Change (RC) of water inflows since 1979/1980; and (d, e, f) Id. for precipitation during Spring, Summer, and Autumn season. The RC is computed as Eq. 2 (Section 2.2). Basically, the RC analysis compares the mean during 1980-2018 with the mean during 1952-1979. Symbols represent positive RC (filled triangle point-up) and negative RC (filled triangle point down), being marked with a black outline the significant estimates. Contours of orography (black) and IHB of continental Spain (purple) were also added (see Fig. 1 of the manuscript).

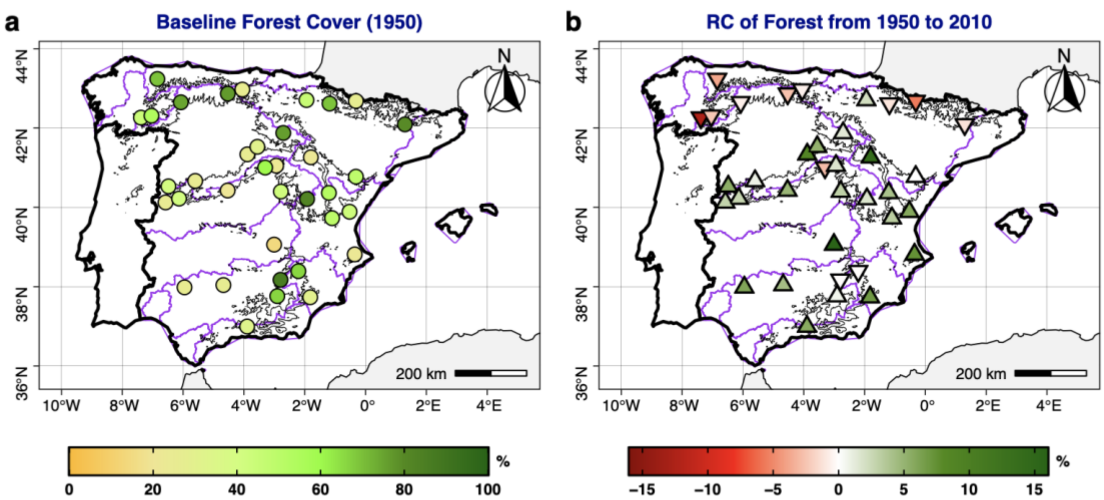

Figure S9. Panels show (a) the percentage of forest cover in 1950 (baseline); and (b) its mean relative change (RC) from 1950 to 2010 computed after Eq. 3. In case of the RC, symbols represent positive RC (filled triangle, point-up) and negative RC (filled triangle, point-down). Contours of orography (black) and IHB of continental Spain (purple) were also added (see Fig. 1 of manuscript).

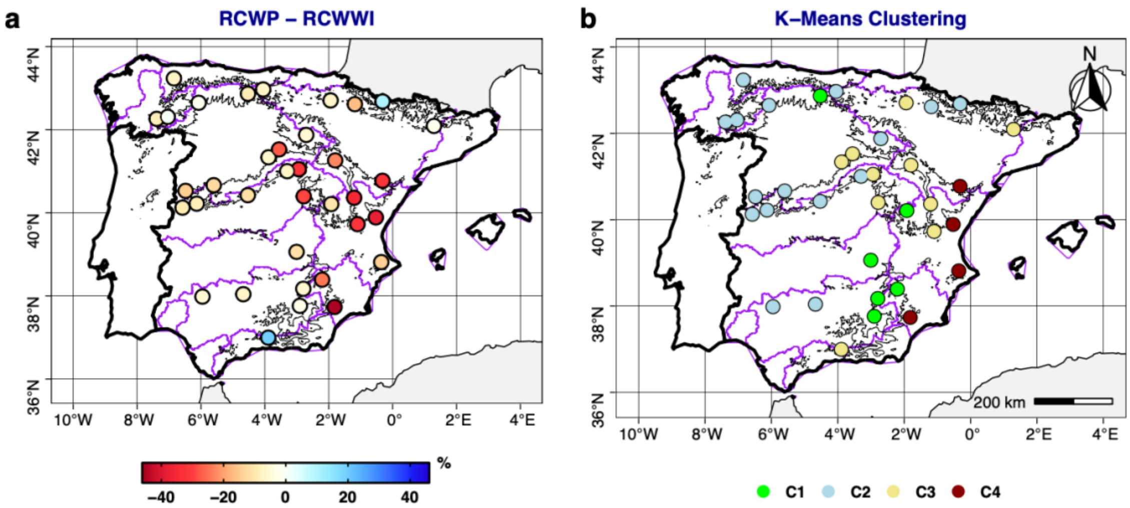

Figure S10. Panels show the difference between RC of WP and RC of WWI (a), and the clustering of catchments through K-Means method (b). Contours of orography (black) and IHB of continental Spain (purple) were also added (see Fig. 1 of manuscript).

Tables

Table S1. Basic details of NENWIRES reservoirs. CR refers to their codes in the manuscript, CROEA refers to their official codes in the Spanish repository of hydrological data (see Section 2.1 in the manuscript), IHB refers to their basins, NAME of reservoirs, LON (longitude) and LAT (latitude), YR refers to the first year of series, VOL refers to their maximum water reserve which can be stored and NMN refers to the altitude (meters above sea level) of their dams.

CR	CROEA	IHB	NAME	LON	LAT	YR	VOL	NMN
R1	2039	DOURO	AGUEDA	-6.48	40.53	1944	22.4	637
R2	9830	EBRO	ALLOZ	-1.94	42.71	1944	66	469
R3	8006	JUCAR	ARQUILLO DE SAN BLAS	-1.20	40.36	1967	21	974
R4	8014	JUCAR	BENAGEBER	-1.10	39.73	1944	221.3	527
R5	8007	JUCAR	BENIARRES	-0.36	38.81	1957	27	318
R6	5021	GUADALQUIVIR	LOS BERMEJALES	-3.89	37.00	1954	102.6	829
R7	5029	GUADALQUIVIR	LA BOLERA	-2.90	37.76	1967	53.2	971
R8	3148	TAGUS	BORBOLLON	-6.58	40.13	1957	88	313
R9	9835	EBRO	BUBAL	-0.32	42.68	1970	62.7	1085
R10	3043	TAGUS	BUENDIA	-2.78	40.40	1954	1639	712
R11	2037	DOURO	BURGOMILLODO	-3.89	41.34	1944	15	874
R12	3111	TAJO	EL BURGUILLO	-4.53	40.42	1944	201	729
R13	1790	MINHO-SIL	CHANDREJA	-7.39	42.26	1958	61	910
R14	2001	DOURO	CUERDA DEL POZO	-2.70	41.88	1946	249	1085
R15	9801	EBRO	EBRO	-4.05	42.97	1945	541	839
R16	7002	SEGURA	FUENSANTA	-2.21	38.39	1944	210	602
R17	3142	TAGUS	GABRIEL Y GALAN	-6.13	40.22	1956	911	386
R18	5062	GUADALQUIVIR	GUADALMELLATO	-4.67	38.04	1944	146.6	212
R19	2036	DOURO	LINARES DEL ARROYO	-3.56	41.53	1951	58	915
R20	9862	EBRO	OLIANA	1.29	42.09	1958	101	518
R21	3065	TAJO	PALMACES	-2.94	41.05	1948	32	885
R22	4001	GUADIANA	PENARROYA	-3.01	39.06	1959	51	735
R23	5011	GUADALQUIVIR	EL PINTADO	-5.95	37.98	1948	212.8	341
R24	1791	MINHO-SIL	PRADA	-7.04	42.31	1960	122	845
R25	7007	SEGURA	PUENTES	-1.82	37.73	1944	29.3	474
R26	8019	JUCAR	REGAJO	-0.53	39.89	1959	6	405
R27	2012	DOURO	RIVECERVERA DE RUESGA	-4.53	42.87	1944	11	1042
R28	1406	CANTABRICO	SALIME	-6.85	43.24	1954	266	225
R29	9818	EBRO	SANTOLEA	-0.32	40.77	1958	43.2	583
R30	2038	DOURO	SANTA TERESA	-5.60	40.67	1954	496	886
R31	8023	JUCAR	LA TOBA	-1.92	40.21	1944	9.7	1156
R32	5001	GUADALQUIVIR	TRANCO DE BEAS	-2.80	38.17	1944	498.2	642
R33	9812	EBRO	LA TRANQUERA	-1.80	41.26	1964	84	685
R34	3050	TAGUS	EL VADO	-3.30	41.00	1949	57	924
R35	2027	DOURO	VILLAMECA	-6.07	42.65	1952	20	1009
R36	9829	EBRO	YESA	-1.18	42.62	1959	447	489

Table S2. Indicators of studied variables within each cluster (C). Columns show the frequency of basins grouped in each cluster (F), the average percentage of permeable soils (PPS), average correlation between WWI and NAOi through the study period (NAOi), the average post-1980 RC of WP (RCWP), average post-1980 RC of WWI (RCWWI), the difference between both those RC (DIFRC), the average post-1980 absolute change of SPEI12 (SPEI12), and average RC of Forest through the study period (RCF).

C	F%	MWP	PPS	NAOi	RCWP	RCWWI	DIFRC	SPEI12	RCF
C1	11.1	164.7	46.2	0.1	2.8	-29.6	-32.4	-0.4	5.1
C2	16.7	355.2	70.1	-0.6	-24.4	-35.2	-10.8	-0.8	2.5
C3	27.8	232.4	40.5	-0.4	-22.7	-40.1	-17.5	-0.9	4.7
C4	44.4	445.2	7.8	-0.5	-20.4	-27.5	-7.1	-0.5	-0.1

References

Bivand, R.: Package ‘rgdal’. Bindings for the 'Geospatial' Data Abstraction Library, CRAN [Package], https://cran.r-project.org/web/packages/rgdal/index.html, 2021.

Hijmans, R.J.: Package ‘raster’: Geographic Data Analysis and Modeling, CRAN [Package], https://cran.r-project.org/web/packages/raster/index.html, 2021.

PSL, NCEP/NCAR Reanalysis 1 Repository [Dataset], available at: https://psl.noaa.gov/data/gridded/data.ncep.reanalysis.html, last access: 9 August 2022.

Schulzweida, U.: CDO user guide, Climate Data Operator [Manual], https://code.mpimet.mpg.de/projects/cdo/embedded/index.html, 2019.